IEPC-97-049

Service Life Assessment for Ion Engines

John R. Anderson*, James E. Polk** and John R. Brophy†

Jet Propulsion Laboratory
California Institute of Technology
Pasadena, California

Assessment of the NSTAR ion engine service life is being accomplished through a combination of long duration testing and probabilistic analyses of the credible failure modes. The methodology developed for service life assessment has been applied to a typical mission profile to estimate the risk of mission failure due to charge-exchange ion erosion of the accelerator grid. The assessment is conducted for the proposed Champollion/DS4 mission. The planned mission involves throttling 4 ion engine over a power range from 2.3 kW to 0.5 kW. The risk of mission failure was assessed for scenarios where two, three or four engines were available to accomplish the mission. The probability for mission failure due to charge-exchange ion erosion of the accelerator grid, was found to be 89% for the 2 engine case, 21% for the 3 engine case, and no failures were recorded during a Monte Carlo simulation using 123,000 trials for the 4 engine case.

Introduction

NASA is currently conducting a program called NSTAR (NASA Solar electric propulsion Technology Application Readiness) to validate xenon ion propulsion technology for use on planetary and commercial spacecraft [1]. A key part of this activity is to validate the service life capability the NSTAR ion engine. To accomplish this the NSTAR program is developing a probabilistic analysis methodology to determine the ion engine failure risk as a function of engine run time. Brophy [2] and Polk [3] have applied this methodology to damage accumulation failure modes. They have computed the probability of structural failure of screen and accelerator grids due to sputtering by discharge chamber plasma ions and due to charge-exchange ion induced erosion, respectively. In their calculations Brophy and Polk assume constant engine operating conditions. This paper describes an extension of this methodology to enable failure risk to be assessed for operation over any specified throttling profile. To illustrate this technique, accelerator grid structural failure probability is computed for the Champollion/DS4 mission profile [4]. The Champollion/DS4 mission is currently planning to rendezvous with a comet and demonstrate the technology required to return a sample of the comet nucleus to Earth.

Probabilistic methods are being employed for this analysis to account for uncertainties associated with parameters used in the model. For example, tolerances on independent parameters which determine ion engine operating conditions are specified for the NSTAR propulsion system. In addition to these independent parameters, many of the dependent parameters in the failure model also have uncertainties associated with them. The probabilistic methodology of Moore, et. al. [5, 6] enables these uncertainties to be treated in a quantifiable manner.

Accelerator Grid Erosion – Structural Failure

Details of the accelerator grid charge-exchange erosion geometry have been described by Polk [7] and Rawlin [8]. In general the accelerator grid fails structurally when the charge-exchange "pits and grooves",

* Member of Technical Staff, Advanced Propulsion Technology Group
** Technical Group Leader, Advanced Propulsion Technology Group
† Group Supervisor, Advanced Propulsion Technology Group

located on the downstream face, wear completely through the grid. It is expected that this will take place first at the center of the grid where the highest erosion rates are observed.

The total mass removed from the downstream face of the accelerator grid, m_f, at the time of structural failure, τ_f, may be estimated by

$$m_f = A_b(1-\phi_a)\rho\, t_a \int_0^{\tau_f} \alpha f_a \, d\tau \qquad (1)$$

where A_b is the active grid area, ϕ_a is the initial accelerator grid open area fraction, ρ is the density of the grid material, t_a is the accelerator grid thickness, α is the fraction of the accelerator grid webbing covered by the pit and grooves erosion pattern, and f_a is accelerator grid mass loss flatness parameter defined as the ratio of average to peak accelerator grid mass loss per unit area.

The rate at which accelerator grid mass is removed by charge-exchange ions, $\dot{m}_e$, is given by

$$\dot{m}_e = \frac{m_g}{e} J_b \vartheta_{ab} \beta Y \lambda_y \qquad (2)$$

where m_g is the mass of an atom of grid material, e is the electron charge, J_b is the ion beam current extracted from the thruster, ϑ_{ab} is the accelerator grid impingement current to beam current ratio, β is the fraction of the measured accelerator grid current which strikes the pits and grooves erosion pattern on the downstream grid surface, Y is the sputter yield at normal incidence for xenon on molybdenum, and λ_y is a parameter which reflects the experimental observation that the net sputter yield for accelerator grids is only a fraction of the sputter yield at normal incidence.

Integrating $\dot{m}_e$ to the time at which the grid fails gives the total mass removed from the accelerator grid at failure. Combining this with Eq. (1) yields

$$1 = \left[\frac{m_g}{e\, A_b\,(1-\phi_a)\,\rho\, t_a}\right] \int_0^{\tau_f} \frac{J_b\, \vartheta_{ab} \beta\, Y\, \lambda_y}{\alpha f_a} \, d\tau \qquad (3)$$

which is used to determine the time τ_f at which accelerator grid structural failure occurs. The terms in the brackets preceding the integral are constants, while the terms in the integrand can vary with ion engine operating conditions. In addition, there are uncertainties associated with each of these terms.

The nominal set points for the independent ion engine operating parameters are tabulated, as a function of power processed by the engine, in Table 1. Sixteen throttle levels denoted by TH16 to TH1 cover the range from maximum power (2.3 kW) to minimum power (0.5 kW), respectively. The parameters which influence accelerator grid erosion are beam current, J_b, and accelerator grid voltage, V_a. The uncertainty associated with the beam current is the ±1% of nominal tolerance specified for the NSTAR propulsion system.

Throttle Level	Screen Voltage (V)	Accelerator Voltage (V)	Beam Current (A)	Neutralizer Keeper Current (A)
TH16	1100	-180	1.74	1.5
TH15	1100	-180	1.64	1.5
TH14	1100	-180	1.56	1.5
TH13	1100	-180	1.47	1.5
TH12	1100	-180	1.37	1.5
TH11	1100	-180	1.27	1.5
TH10	1100	-180	1.17	1.5
TH9	1100	-180	1.08	2
TH8	1100	-180	0.98	2
TH7	1100	-150	0.88	2
TH6	1100	-150	0.78	2
TH5	1100	-150	0.68	2
TH4	1100	-150	0.59	2
TH3	1100	-150	0.5	2
TH2	850	-150	0.5	2
TH1	650	-150	0.48	2

Throttle Level	Power (kW)	Main Flow Rate (sccm)	Cathode Flow Rate (sccm)	Neutralizer Flow Rate (sccm)
TH16	2.3	23.62	3.7	3.7
TH15	2.18	22.28	3.42	3.42
TH14	2.06	21.43	3.03	3.03
TH13	1.94	20.19	2.95	2.95
TH12	1.82	18.99	2.72	2.72
TH11	1.7	17.59	2.6	2.6
TH10	1.58	16.07	2.6	2.6
TH9	1.46	14.63	2.6	2.6
TH8	1.34	13.01	2.6	2.6
TH7	1.22	11.49	2.6	2.6
TH6	1.1	9.95	2.6	2.6
TH5	0.98	8.42	2.6	2.6
TH4	0.86	7.2	2.6	2.6
TH3	0.74	5.48	2.6	2.6
TH2	0.62	5.48	2.6	2.6
TH1	0.5	5.48	2.6	2.6

Table 1. Nominal Ion Engine Set Points

The accelerator grid voltage affects the sputter yield, Y, which is calculated from the data of Rosenberg and Wehner [9]. A quadratic curve fit to their data yields

$$Y = -0.1935 + 2.622\text{x}10^{-3}E - 9.97\text{x}10^{-7}E^2 \quad (4)$$

where E is the kinetic energy of the ion striking the downstream surface of the accelerator grid. The kinetic energy of singly charged ions is given by

$$E = |V_a| + V_g + V_{bp} \quad (5)$$

where $|V_a|$ is the magnitude of the accelerator grid voltage, V_g is the coupling voltage and V_{bp} is the potential of the beam plasma with respect to the ambient space plasma (if in space) or facility ground (for ground tests). Nominal values of V_a are given in the throttling table; these have an uncertainty of ±5% of nominal specified for the NSTAR propulsion system. The ranges for the coupling voltage, V_g, (11 to 15 V) and for the beam potential, V_{bp} ,(4 to 10 V) are those used in Ref. 2.

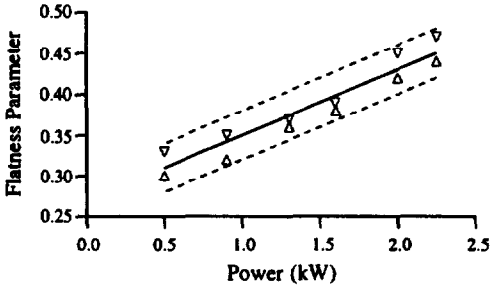

Fig. 1 LDT Flatness Parameter Data

The accelerator grid mass loss flatness parameter, f_a, is assumed to be equal to the ion beam current flatness parameter [2, 3]. Fig. 1 shows the extreme values of the ion beam flatness parameter measured across the grids of the NSTAR engine as a function of power during the 8,000 hour, long duration test (LDT) [10]. A linear curve fit to these data yields

$$f_a = 0.27 + 0.08P \quad (6)$$

where P is the power processed by the ion engine in kW. The line obtained from this function is the solid line in Fig. 1. Also shown are dashed lines bounding the data on the upper and lower sides which are obtained by adding or subtracting a constant uncertainty of 0.03, respectively.

The extreme values for the ratio of accelerator current to beam current ϑ_{ab} obtained during the NSTAR LDT are shown in Fig. 2. The function used to describe these data

$$\vartheta_{ab} = \begin{cases} 6.5\text{x}10^{-4} + P/600 & \text{for } P > 0.9 \\ 2.15\text{x}10^{-3} & \text{for } P < 0.9 \end{cases} \quad (7)$$

is plotted as the solid line in Fig. 2. The dashed lines providing upper and lower bounds to the data were obtained by adding or subtracting 0.001 to ϑ_{ab}, respectively.

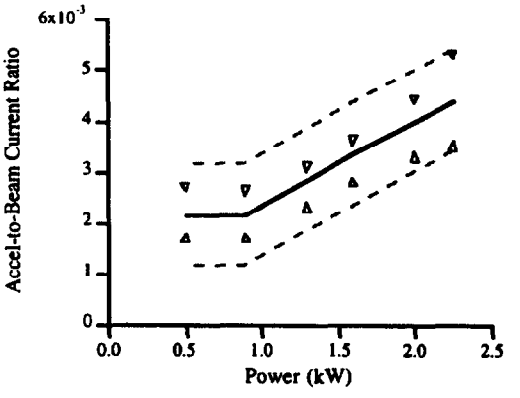

Fig. 2 LDT ϑ_{ab} Data

The remaining three variables α, λ_y, and β have not been characterized as well as the other variables in the integrand. More work is needed and is being conducted [11] to determine how these parameters vary with ion engine operating conditions. Although existing data are sparse, estimates of parameter values based on these data are used for this analysis.

Approximate values for the eroded area fraction, α, were obtained from photographs taken of three accelerator grids used during tests conducted under the NSTAR program [11-13]; it is believed to be in the range 0.30 to 0.46. Since these tests were conducted at full power, it is not known how α varies with power.

Values for net sputter yield, λ_y, of 0.37 to 0.50 are those used in Ref. 2. Although

ion energy does influence the net sputter yield, it is thought to be primarily affected by redeposition effects in the pits and grooves pattern. If this is the case, its value should not vary significantly with power level.

The fraction of accelerator grid impingement current, β, striking the pits and grooves is estimated to be between 0.7 and 0.9. This range is thought to be conservative, since smaller values would give lower erosion rates. In Ref. 2, it is argued that 0.75 might be a reasonable estimate of the value of this parameter.

In addition to determining the time to accelerator grid failure, it is also of interest to determine the amount of propellant that a thruster processes before it fails. The mass processed by an ion engine before failure M_f is given by

$$M_f = \int_0^{\tau_f} (M_m + M_c + M_n)\, d\tau \qquad (7)$$

where M_m is the main flow rate, M_c is the cathode flow rate and M_n is the neutralizer flow rate. The uncertainty associated with these flow rates is the ±3% of nominal tolerance specified for the NSTAR propulsion system.

Results - Constant Power

Prior to presenting the mission analysis, the effect of power level on the amount of propellant mass processed before grid failure is discussed. To illustrate this effect, erosion model equations were solved for various throttle levels with the power held constant. This was done using a Monte Carlo simulation with 32,000 trials to generate probability distributions for mass processed before grid failure, assuming uniformly distributed uncertainties for each of the parameters over their respective ranges.

Distributions for 5 levels ranging from maximum to minimum power are shown in Fig. 3. As power level decreases flatness parameter, mass flow rate, beam current and the ratio of accelerator grid impingement current to beam current all decrease. Decreases in flatness parameter (resulting in higher erosion at the center relative to the rest of the grid) and in mass flow rate tend to reduce the mass that a thruster processes before grid failure. However, decreases in beam current and in the ratio of accelerator grid impingement current to beam current tend to reduce the overall erosion rate. As seen in Fig. 3, the latter two effects dominate and the amount of propellant mass processed before grid failure increases as power decreases.

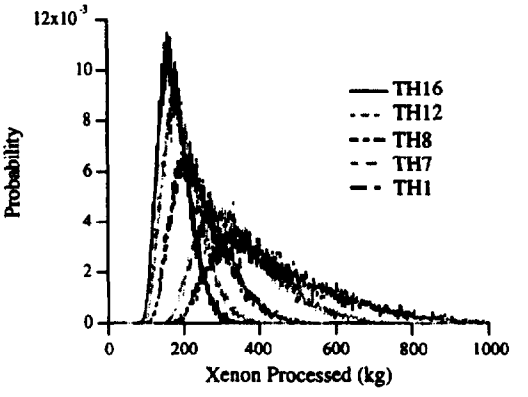

Fig. 3. Xenon Processed Before Accelerator Grid Structural Failure

In addition to this trend, there is a jump in mass processed between throttle levels Th8 and Th7. This occurs because of decreased erosion rates resulting from decreased ion energies as the magnitude the accelerator grid voltage is reduced from 180 to 150 V. Also, the tendency for the distributions to skew toward large values at lower power levels is caused predominantly by the uncertainty in the accelerator grid to beam current ratio.

The curves in Fig. 3 can be integrated to obtain the probability that accelerator grid failure will occur before a specified amount of mass is processed. This was done for all power levels in Table 1 and the B10 and B50 lives are plotted in Fig. 4. Here the Bn life is defined as the amount of mass the engine will have processed when the probability of accelerator grid failure is n%.

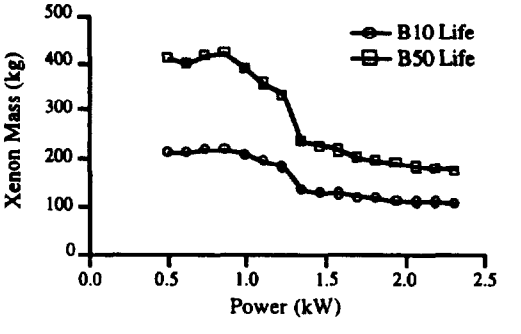

Fig. 4 Propellant Mass Processed at Constant Power

It is of interest to compare results of these calculations with data from the NSTAR LDT test. The NSTAR 30-cm ion engine has processed ~75 kg of xenon and ~10% of the mass required to cause structural failure has been eroded during the first 7,000 hours of the LDT [11]. The LDT neutralizer flow rate was 3.0 sccm instead of 3.7 sccm used in the simulation. Accounting for this difference and linearly extrapolating the erosion rate until accelerator grid failure would result in the engine processing ~750 kg. This exceeds the maximum of 658 kg computed using the extreme values for the parameters in Eq. 3. It is noted, however, that the erosion rates observed during the LDT may be artificially low due to backsputtered facility carbon deposition on the accelerator grid. Further work is needed to determine what differences facility related effects cause in grid erosion from that which would be observed in space.

Results - Mission Throttling Profile

The Champollion/DS4 mission has several powered segments during which either one or two ion engines are operated. For this analysis, it is assumed that there is a primary and a secondary engine. The primary engine is used during all powered segments of the mission. The secondary engine is used only during the portions of the mission where two engines are operating. The power throttle profile for the primary and secondary engines are shown in the lower and upper graphs of Fig. 5, respectively. The primary engine operates during four powered periods; the first two segments are at high power levels and result in more erosion damage than the last two lower power segments. The secondary engine operates for two powered segments; high erosion rates are expected during these segments because of the high power levels.

To successfully complete the Champollion/DS4 mission at nominal operating conditions, 442 kg of xenon must be processed, 292 and 150 kg by the primary and secondary engines, respectively. The total mass to be processed is equivalent to the full power B10 life of four engines; Champollion/DS4 is planning to use four ion engines. The individual engines will be referred to as engine 1, engine 2, engine 3, and engine 4. At the beginning of the mission engine 1 and engine 2 will be used as the primary and secondary engines, respectively. If the primary engine fails the secondary engine becomes the primary engine and one of the spares becomes the secondary engine. Engine 3 will be the first spare engine to be used. If the secondary engine fails, one of the spare engines becomes the secondary engine. For example, if engine 2 fails before engine 1, engine 3 becomes the secondary engine. If engine 1 subsequently fails, engine 3 becomes the primary engine and engine 4 becomes the secondary engine.

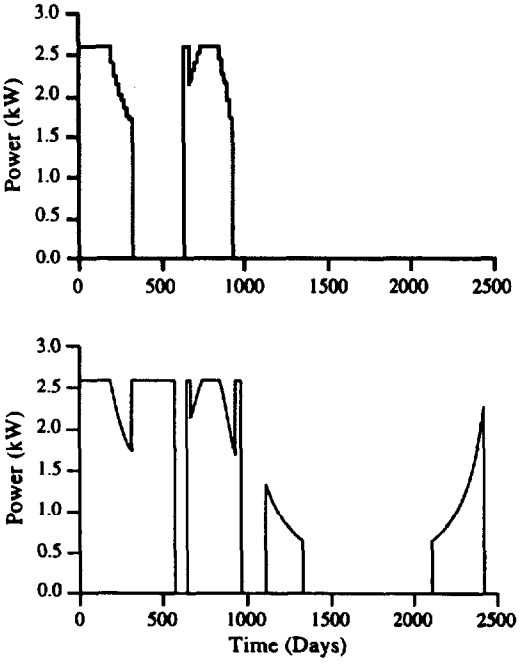

Fig. 5 Power Profile for Champollion/DS4

Probability distribution functions of accelerator grid structural failure for individual engines were computed; to obtain these distributions, a Monte Carlo simulation with 123,000 trials was run. These probability distribution functions are plotted as a function of mission time in Fig. 6. The gaps in the distribution occur because the probability of failure is zero when the engines are not operating. Integrating these distributions gives the probability that a particular engine will suffer accelerator grid structural failure before a given time in the mission. These probabilities are shown in Fig. 7.

Because the primary engine operates for longer periods than the secondary engine, engine 1 is likely to fail before engine 2. Engine 1 is most likely to fail during the second powered segment of the primary engine power profile, although it can fail late in the first powered segment. The probability of failure for engine 1 decreases during the last two powered segments in part because the

engine is operating at lower power levels and in part because these segments fall in the long life tail of its failure distribution. The probability that engine 1 will have suffered accelerator grid failure by the end of the mission is 0.955.

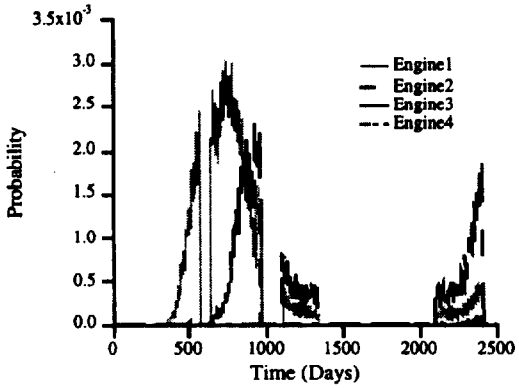

Fig. 6 Probability Distribution for Accelerator Grid Failure

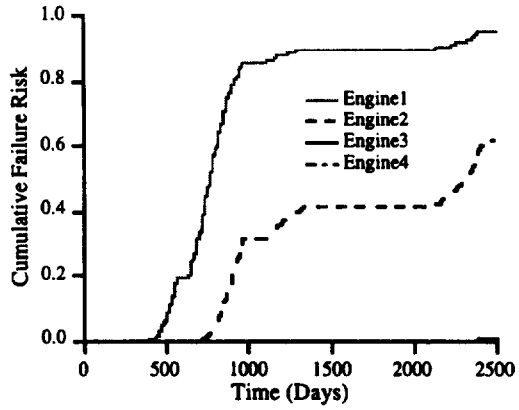

Fig. 7 Cumulative Risk for Accelerator Grid Failure

Because the powered segments for the secondary engine are shorter duration than those for the primary engine, engine 2 is unlikely to fail until late in the secondary engine power profile or until it has become the primary engine. Engine 2 has a higher probability of failing in the last two powered segments of the mission than Engine 1 because it processes less mass during the first two powered segments. The probability that engine 2 will fail during the mission is 0.613.

Since engines 1 and 2 do most of the thrusting during the high powered segments of the mission, engine 3 is unlikely to fail until late in the mission. The probability of accelerator grid failure for engine 3 is 0.004 at the end of the mission.

Although engine 4 might have to be used for some portion of the mission, the other engines complete most of the thrusting. Therefore, it is unlikely that engine 4 will have accumulated enough run time to be at the end of its life during this mission. Out of the 123,000 cases run during the simulation no accelerator grid failures of engine 4 were recorded.

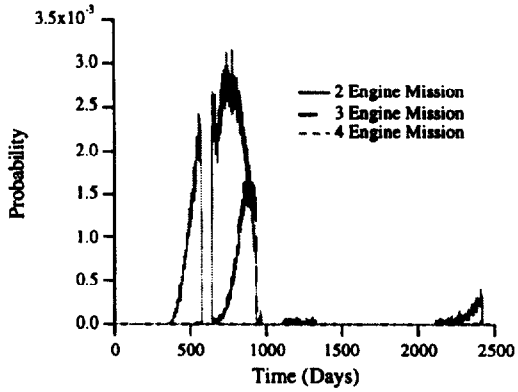

Fig. 8 Probability Distribution for Mission Failure

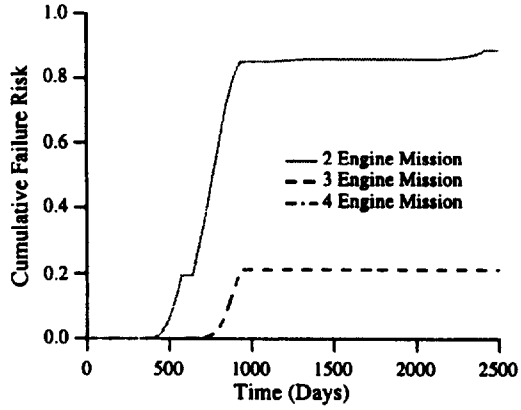

Fig. 9 Cumulative Distribution for Mission Failure

For mission planning it is of interest to determine how the risk of mission failure is influenced by the number of engines installed on the spacecraft. To investigate this, the failure risk was computed for cases where 2, 3 or 4 engines were available to conduct the mission. The probability distribution function for risk of mission failure is shown in Fig. 8. These functions are integrated to obtain the probability that accelerator grid structural failure will cause mission failure by a

particular time. The integrated curves are shown in Fig. 9.

For the N engine case (here N=2, 3, or 4), mission failure occurs if N-1 engines fail before the secondary engine power profile is completed. After completion of the secondary engine profile, failure of all N engines is required to cause mission failure. As a result the failure probability distribution is highest before completion of the secondary engine profile and then decreases to lower values.

The probability of mission failure is 0.888 for the case where only 2 engines are used. As noted this is primarily due to the high likelihood that at least one engine will fail before completion of the secondary engine power profile.

For the 3 engine case the probability of mission failure is 0.213. Again, the risk is dominated by the probability that 2 of the 3 engines will fail before the secondary engine completes its mission.

With 4 engines, no mission failures were recorded in the 123,000 cases run. Because of the relatively high risk of failure incurred by reducing the number of engines, it is recommended that 4 engines be used for the Champollion/DS4 mission.

Although it was not considered in this analysis, Champollion/DS4 may impose an additional restriction on the power throttling profile [14]. Due to constraints imposed by the propulsion module gimbaling system, ion engines may have to be paired when two engines are operating. This may be required to maintain the thrust vector through the spacecraft center of gravity. Therefore, if one engine of a pair fails, the other pair must be used to complete the two engine power profile.

This constraint increases the risk of mission failure because it restricts the choice of engines which can be used during the two engine phase of the mission. Additional work is planned to determine how this constraint impacts the risk of mission failure. If this planned analysis were to reveal a large increase in risk to the mission, a redesign of the gimbaling system might be warranted.

Conclusions

Probabilistic modeling techniques developed to determine failure mode distributions for ion engines operating at constant power levels have been extended to determine failure probabilities for missions with time varying operating conditions. One particular failure mode--accelerator grid structural failure due to charge-exchange ion erosion--was examined for the Champollion/DS4 mission. The analysis presented here indicates that this failure mode does not pose a serious risk to the mission if, as currently planned, 4 ion engines are used.

Acknowledgments

The research described in this paper was conducted at the Jet Propulsion Laboratory, under a contract with the National Aeronautics and Space Administration.

References

1. Casani, E. K. and Lehman, D. H., "Deep Space One Memorandum of Agreement," Interoffice Memorandum, DS1-DHL-96-012, May 24, 1996, Internal JPL Document.
2. Brophy, J. R., Polk, J. E. and Rawlin, V. K., "Ion Engine Service Life Validation by Analysis and Testing," AIAA-96-2715, presented at the 32nd AIAA/ASME/SAE/ASEE Joint Propulsion Conference, Lake Buena Vista, FL, July 1996.
3. Polk, J. E., et.al., "Probabilistic Analysis of Ion Engine Accelerator Grid Life," IEPC-93-176, presented at the 23rd International Electric Propulsion Conference, Seattle, WA, Sept. 1993.
4. Muirhead, B., "Champollion/DS-4 Mission Overview," report to the NASA Associate Administrator for Space Science, April 15, 1997.
5. Moore, N., Ebbler, D., and Creager, M., "Probabilistic Service Life Assessment," in Reliability Technology-1992, Vol. AD-28, American Society of Mechanical Engineers, 1992. ISBN 0-7918-1095-X
6. Moore, N., et. al., "An Improved Approach for Flight Readiness Assessment-Methodology for Failure Risk Assessment and Application Examples," JPL 92-15, Jet Propulsion Laboratory, California Institute of technology, Pasadena, CA, 1992.
7. Polk, J. E., Brophy, J. R., and Wang, J., "Spatial and Temporal Distribution of Ion Engine Accelerator Grid Erosion," AIAA-95-2924, presented at the 31st Joint Propulsion Conference, San Diego, CA, July 1995.

8. Rawlin, V. K., "Erosion Characteristics of Two-Grid Ion Accelerating Systems," IEPC-93-175, presented at the 23rd International Electric Propulsion Conference, Sept. 1993.
9. Rosenberg, D., and Wehner, G. K., "Sputtering Yields for Low Energy He^+-, Kr^+-, and Xe^+-Ion Bombardment," *Journal of Applied Physics*, Vol. 33, No. 5, May 1962.
10. Sovey, J. S., "Development of an Ion Thruster and Power Processor for New Millennium's Deep Space 1 Mission," AIAA-97-2778, presented at the 33rd AIAA/ASME/SAE/ASEE Joint Propulsion Conference, Seattle, WA, July 1997.
11. Polk, J. E., et. al., "In Situ, Time-Resolved Accelerator Grid Erosion Measurements in the NSTAR 8000 hr Endurance Test", IEPC-97-047 to be presented at the 25th International Electric Propulsion Conference, Cleveland, OH, August 1997.
12. Patterson, M. J., et. al., "2.3-kW Ion Thruster Wear Test," AIAA-95-2516, presented at the 31st AIAA/ASME/SAE/ASEE Joint Propulsion Conference, San Diego, CA, July 1995.
13. Polk, J. E., et. al., "A 1000-Hour Wear Test of the NASA 30-cm Xenon Ion Engine," AIAA-96-2717, presented at the 32nd Joint Propulsion Conference, Lake Buena Vista, FL, July 1996.
14. Tan-Wang, G. H., Private Communication, August 1997.